Transmission line equivalent circuit model applied to a plasmonic grating nanosurface for light trapping

Alessia Polemi and Kevin L. Shuford*

Department of Chemistry, Drexel University, 3141 Chestnut Street, Philadelphia, PA 19104, USA

**shuford@drexel.edu*

Abstract: In this paper, we show how light absorption in a plasmonic grating nanosurface can be calculated by means of a simple, analytical model based on a transmission line equivalent circuit. The nanosurface is a one-dimensional grating etched into a silver metal film covered by a silicon slab. The transmission line model is specified for both transverse electric and transverse magnetic polarizations of the incident light, and it incorporates the effect of the plasmonic modes diffracted by the ridges of the grating. Under the assumption that the adjacent ridges are weakly interacting in terms of diffracted waves, we show that the approximate, closed form expression for the reflection coefficient at the air-silicon interface can be used to evaluate light absorption of the solar cell. The weak-coupling assumption is valid if the grating structure is not closely packed and the excitation direction is close to normal incidence. Also, we show the utility of the circuit theory for understanding how the peaks in the absorption coefficient are related to the resonances of the equivalent transmission model and how this can help in designing more efficient structures.

OCIS codes: (160.4760) Optical properties; (240.6680) Surface plasmons; (050.1960) Diffraction theory.

References and links

1. H. A. Atwater and A. Polman, "Plasmonics for improved photovoltaic devices," Nature Mater. **9**, 205–213 (2010).
2. A. Tiwari, A. Romeo, D. Bätzner, and H. Zogg, "Flexible CdTe solar cells on polymer films," Prog. Photovolt: Res. Appl. **9**, 211–215 (2001).
3. A. Romeo, A. Terheggen, D. Abou-Ras, D. L. Bätzner, F.-J. Haug, M. K. D. Rudmann, and A. N. Tiwari, "Development of thin-film Cu(In,Ga)Se2 and CdTe solar cells," Prog. Photovolt: Res. Appl. **12**, 93–111 (2004).
4. W. Koch, A. Endrös, D. Franke, C. Häbler, J. P. Kaleis, and H.-J. Möller, "Bulk crystal growth and wavering for PV," *Handbook of Photovoltaic Science and Engineering*, pp. 205–255 (John Wiley 2003).
5. V. E. Ferry, J. N. Munday, and H. A. Atwater, "Design considerations for plasmonic photovoltaics," Adv. Mater. **22**, 4794–4808 (2010).
6. P. N. Saeta, V. E. Ferry, D. Pacifici, J. N. Munday, and H. A. Atwater, "How much can guided modes enhance absorption in thin solar cells?" Opt. Express **17**, 975–20, (2009).
7. V. E. Ferry, L. A. Sweatlock, D. Pacifici, and H. A. Atwater, "Plasmonic nanostructure design for efficient light coupling into solar cells," Nano Lett. **8**, 4391–4397 (2008).
8. M. Green, *Third generation photovoltaics: advanced solar energy conversion*, Springer series in photonics (Springer, 2003). URL http://books.google.com/books?id=TimK46htCMoC.
9. D. Madzharov, R. Dewan, and D. Knipp, "Influence of front and back grating on light trapping in microcrystalline thin-film silicon solar cells," Opt. Express **19**, 95–107 (2011).

#157235 - $15.00 USD Received 28 Oct 2011; revised 13 Dec 2011; accepted 16 Dec 2011; published 2 Jan 2012

10. R. A. Pala, J. White, E. Barnard, J. Liu, and M. L. Brongersma, "Design of plasmonic thin-film solar cells with broadband absorption enhancements," Adv. Mater. **21**, 3504–3509 (2009).
11. A. Polyakov, S. Cabrini, S. Dhuey, B. Harteneck, P. J. Schuck, and H. A. Padmore, "Plasmonic light trapping in nanostructured metal surfaces," Appl. Phys. Lett. **98**, 104–107 (2011).
12. C. Haase and H. Stiebig, "Optical properties of thin-film silicon solar cells with grating couplers," Prog. Photovolt: Res. Appl. **14**, 629–641 (2006).
13. K. Yee, "Numerical solution of initial boundary value problems involving Maxwell's equations in isotropic media," IEEE Trans. Antennas Propag. **14**, 302–307 (1966).
14. T. Weiland, "A discretization method for the solution of Maxwell's equations for six-component fields," Electron. Commun. **31**, 116–120 (1977).
15. N.-N. Feng, J. Michel, L. Zeng, J. Liu, C.-Y. Hong, L. C. Kimerling, and X. Duan, "Design of Highly Efficient Light-Trapping Structures for Thin-Film Crystalline Silicon Solar Cells," IEEE Trans. Electron Devices **54**, 1926–1933 (2007).
16. J. Chen, Q. Wang, and H. Li, "Microstructured design of metallic diffraction gratings for light trapping in thin-film silicon solar cells," Opt. Commun. **283**, 5236–5244 (2010).
17. M. G. Moharam and T. K. Gaylord, "Rigorous coupled-wave analysis of planar-grating diffraction," J. Opt. Soc. Am. A **71**, 811–818 (1981).
18. T. Tamir and S. Zhang, "Modal transmission-line theory of multilayered grating structures," J. Lightwave Technol. **14**, 914–927 (1996).
19. A. Chutinan and S. John, "Light trapping and absorption optimization in certain thin-film photonic crystal architectures," Phys. Rev. A **78**, 023,825 (2008).
20. Z. Yu, A. Raman, and S. Fan, "Fundamental limit of light trapping in grating structures," Opt. Express **18**, 366-380 (2010).
21. I. T. A. Luque and A. Marti, "Light intensity enhancement by diffracting structures in solar cells," J. Appl. Phys. **104**, 502–034, (2008).
22. L. Felsen and N. Markuvitz, *Radiation and scattering of waves*, 1st ed. (Prentice-Hall, Englewood Cliffs, NJ, 1973).
23. www.cst.com (2011 CST Computer Simulation Technology AG).
24. E. Palik, *Handbook of optical constants of solids*, 1st ed. (Academic Press, Orlando, 1985).
25. A. Polemi, A. Toccafondi, and S. Maci, "High-frequency Green's function for a semi-infinite array of electric dipoles on a grounded slab. Part I: formulation," IEEE Trans. Antennas Propag. **49**, 1667–1677 (2001).
26. B. Davies, "Locating the zeros of an analytic function," J. Comput. Phys. **66**, 36–49 (1986).

1. Introduction

Light trapping is an optical phenomenon that many photovoltaic cells employ to increase performance. The design and fabrication of novel optical components that can improve light trapping capability is essential to achieve higher efficiencies in photovoltaic devices [1]. In recent years, researchers have investigated several architectures to accomplish this goal including the use of different semiconductor materials, such as cadmium telluride and copper indium gallium arsenide, which have produced record efficiencies [2, 3]. Unfortunately, these materials are scarce in nature; thus, the dominant commercial solar material, silicon (Si), is still most relevant. Silicon is a weak absorber in much of the optical regime, requiring at least $200-300\mu m$ of material thickness to completely absorb incident sunlight [4, 5]. For crystalline Si, 50% of the cell cost is due to the cost of material itself [4], which suggests the film could be made thinner to substantially decrease cost. However, the energy trapped and converted into photocurrent is in fact proportional to the number of cavity modes supported by the semiconductor film [6, 7]. As a general guideline, the higher the number of modes, the higher the absorption of the incident light in the semiconductor. The number of modes is dictated primarily by the thickness of the semiconductor layer. In particular, the number of modes supported increases with the thickness of the film, which implies higher material costs. Also, for thick films, due to the long path length of the photonic modes, the electron-hole recombination rate increases [3]. As a consequence, the photocurrent available for conversion decreases, diminishing the solar cell efficiency. For these reasons, the tradeoff between keeping the cost of semiconductors low and providing a high degree of absorption must be achieved in a different way.

The recent trend in photovoltaics is to fabricate solar cells with a thin semiconductor film [8],

#157235 - $15.00 USD Received 28 Oct 2011; revised 13 Dec 2011; accepted 16 Dec 2011; published 2 Jan 2012

and, at the same time, to increase the optical path length by increasing the light scattering process inside the semiconductor. Incorporation of plasmonic nanostructures into photovoltaic devices has been demonstrated as a viable pathway to achieve these goals [1,7,9]. One of the most common plasmonic structures employed to reduce the physical thickness of the film material is a 1-D corrugated metallic film on the back surface of a thin photovoltaic absorber layer. This grating structure can couple sunlight into Surface Plasmon Polariton (SPP) modes supported at the metal-semiconductor interface as well as into cavity modes in the semiconductor slab (also called photonic or guided modes). This structure has been investigated previously using numerical methods [10–12], namely Finite Difference Time Domain [13], Finite Integration Techniques [14], and semi-analytical methods based on Rigorous Coupled Wave Analysis [15–17] and Modal Transmission Line theory [18]. Recently, researchers have also developed analytical methods [19–21] to analyze different aspects of the light trapping mechanism supported by a corrugated metallic film. In Ref. [20] for example, the authors develop a statistical temporal coupled mode theory formalism to study the limit of absorption for grating structures. An interesting simplified three-dimensional model is presented in Ref. [21], based on the theory of periodic radiation arrays and applied to one- and two-dimensional diffraction gratings. The authors apply the approximated model to investigate the scattering direction and the path length enhancement in diffraction gratings.

In the framework of the analytical methods, we show in this paper how a simple transmission line equivalent circuit theory [22] can be applied to calculate the absorption coefficient of the solar cell. The transmission line model is characterized for both polarizations of the incident light, transverse electric (TE) and transverse magnetic (TM). We consider a grating structure composed of a Si film that covers a silver (Ag), 1-D corrugated back surface. We show that if the adjacent ridges of the grating are not strongly coupled, the approximate, closed form expression for the reflection coefficient at the air-Si interface can be used to evaluate the light absorption of the solar cell. The weak-coupling assumption is valid if the grating structure is not closely packed and if the impinging light is arriving from a direction close to normal incidence. Even with these constraints, the circuit theory results are useful to understand how the peaks in the absorption coefficient are related to the resonances of the equivalent transmission model. In fact, we show that the maximum absorption occurs when the equivalent impedance at the air-Si interface acts as on open circuit condition, which from the electromagnetic point of view is equivalent to a perfect magnetic conductor (PMC) condition. Under this condition, the tangential component of the electric field is maximum, thus justifying the maximum of absorption within the Si slab. The specific condition is dictated by the cavity mode resonances and by their interaction with both diffraction and plasmonic modes. This information can be used to design efficient grating nanosurfaces with multiple open circuit conditions or broader bandwidth resonances by optimizing the equivalent impedance retrieved at the interface.

The paper is organized as follows. In Section 2, we apply the transmission line model to the simple case of a flat, Ag-Si cell and demonstrate how to calculate the absorption through the circuit theory. Also, we show the dispersion diagram of the solar cell, obtained by means of the relevant Green's function, emphasizing the number of cavity (photonic) modes and the TM-plasmonic mode. In Section 3, we apply the same model to the 1-D grating nanosurface, characterizing both TE and TM polarization. We show how to modify the model by applying the circuit theory based on the conservation of the tangential components of the electromagnetic field at the junction between the ridge zone and the flat zone of the grating. This leads to a shunt connection for TE fields and to a series connection for TM fields. Also, we demonstrate how to include an extra load in the circuit, which represents the plasmonic near field accumulation around the ridge of the grating. The absorption coefficient is calculated and compared with a full wave simulation using CST Microwave Studio [23]. The model is also applied to the same

#157235 - $15.00 USD Received 28 Oct 2011; revised 13 Dec 2011; accepted 16 Dec 2011; published 2 Jan 2012

structure covered by an antireflecting coating of TiO_2. In Section 4, we present the absorption enhancement with respect to a flat metallic film solar cell. In particular, we demonstrate how the circuit theory allows us to interpret the peaks in the absorption spectrum in terms of an equivalent open circuit condition at the air-Si interface, which can be used as a guideline to design more efficient structures.

2. Plasmonic modes and photonic modes

We first develop the transmission line model for a single solar cell arrangement composed of a flat, Ag film covered by a Si slab of height h, as shown in Fig. 1(a). The thickness of the Ag film is larger than the skin depth. The optical constants of Ag and Si have been taken from Ref. [24]. When the light strikes the solar cell, part of the energy is trapped inside the Si slab. The number and the nature of the excited modes inside the Si slab can be calculated by means of the spectral domain Green's function (GF) of the structure. The GF singularities represent

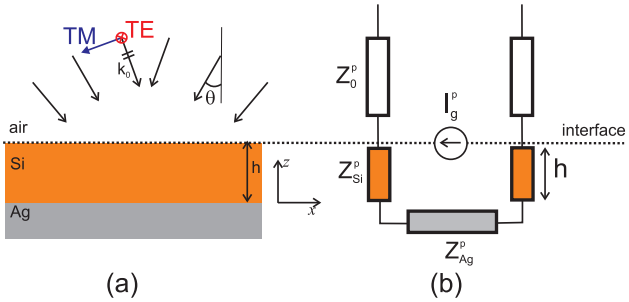

Fig. 1. (a) Reference geometry for a flat metallic film solar cell. (b) Equivalent transmission line (p=TM,TE)

the modes supported by the Si slab [22, 25]. The spectral GF can be calculated in a closed form by resorting to an equivalent transmission line model along the longitudinal direction (z), as shown in Fig. 1(b). The transmission line source is assumed to be fed by an elementary point source placed at the interface between air and Si (I_g in Fig. 1(b)). This spectral point source (i.e. elementary dipole) represents the expansion of all plane waves impinging on the structure from all possible directions [22], and additionally, it acts as the current generator of the equivalent electric circuit. The model is valid for both TM and TE polarization by simply selecting the correct representation of the modal impedances along the transmission line. In particular,

$$Z_X^{TM}(k_t) = \xi_X \frac{\sqrt{k_X^2 - k_t^2}}{k_X} \tag{1a}$$

$$Z_X^{TE}(k_t) = \xi_0 \frac{k_0}{\sqrt{k_X^2 - k_t^2}} \tag{1b}$$

where $X = 0$ in air, $X = Si$ in silicon, and $X = Ag$ in the silver. In the above equations, $\xi_X = \xi_0/n_X$ represents the characteristic impedance of the material, expressed in terms of the free space characteristic impedance ξ_0 and the refractive index of the medium n_X. Analogously, $k_X = n_X k_0$ represents the wavenumber in the material with k_0 being the free space wavenumber. The spectral dependence is taken into account through the transverse wavenumber $k_t = \sqrt{k_X^2 - k_{zX}^2}$, which is invariant along the interfaces. In fact, k_t represents the component of the incoming light wavevector that is parallel to the interface. This component is required to

#157235 - $15.00 USD Received 28 Oct 2011; revised 13 Dec 2011; accepted 16 Dec 2011; published 2 Jan 2012

be constant according to Snell's laws. At the air-Si interface, the equivalent impedance for both TM and TE polarizations can be calculated as

$$Z_{int}^{p} = Z_{Si}^{p} \frac{Z_{Ag}^{p} + jZ_{Si}^{p} \tan\left(h\sqrt{k_{Si}^{2} - k_{t}^{2}}\right)}{Z_{Si}^{p} + jZ_{Ag}^{p} \tan\left(h\sqrt{k_{Si}^{2} - k_{t}^{2}}\right)} \tag{2}$$

where p =TM,TE. All the impedances in Eq. (2) are variables of k_t. From hereinafter, this dependence is considered understood and suppressed for simplicity of notation. The spectral GF associated with the electric field can be now calculated as the equivalent voltage at the interface where the point source is located [22]. This leads to the following implicit expression

$$GF^{p} = I_{g}^{p} \frac{Z_{0}^{p} Z_{int}^{p}}{Z_{0}^{p} + Z_{int}^{p}} \tag{3}$$

where the constant I_g can be set to 1 without lack of generality. In general, I_g is proportional to the dipole momentum $I\delta$, where I is current flowing in a dipole of length δ. Since we are looking at the dispersion, the amplitude of the generator is not crucial. By inserting Eq. (2) into Eq. (3), we then obtain

$$GF^{p} = \frac{Z_{0}^{p} Z_{Si}^{p} \left[Z_{Ag}^{p} + jZ_{Si}^{p} \tan\left(h\sqrt{k_{Si}^{2} - k_{t}^{2}}\right)\right]}{\left[Z_{Si}^{p}\left(Z_{0}^{p} + Z_{Ag}^{p}\right) + j\left(Z_{0}^{p} Z_{Ag}^{p} + {Z_{Si}^{p}}^{2}\right) \tan\left(h\sqrt{k_{Si}^{2} - k_{t}^{2}}\right)\right]} \qquad p = \text{TM,TE} \tag{4}$$

where the formulas in Eq. (1) can be used for each impedance to obtain an explicit TM and TE spectral GF expression.

By investigating the spectral GF, we note that the denominator of Eq. (4) shows singularities in terms of the variable k_t. These singularities can be calculated by using a complex zeros searching routine. In the present case, a Fortran 90 routine has been customized based on Ref. [26]. The singularities of the spectral GF allow us to understand the typology of modes supported by the flat metallic film solar cell. There are two main categories: cavity modes and one SPP mode supported at the interface between the metal film and the Si slab. The cavity modes are found by searching for the singularities for which $k_0 < Re\{k_t\} < Re\{k_{Si}\}$, and by adding an imaginary part that is proportional to $Im\{k_{Si}\}$ in order to account for the losses. The starting point that we used in the present routine is $k_t = (Re\{k_{Si}\} + k_0)/2$. The SPP mode is found by using the same zeros searching routine but by changing the starting point. In this case, we use the value of k_t associated with the solution for the ideal case of an interface between two semi-infinite media, i.e.

$$k_t = k_0 \sqrt{\frac{\varepsilon_{Si}\varepsilon_{Ag}}{\varepsilon_{Si} + \varepsilon_{Ag}}} \tag{5}$$

where ε_{Si} and ε_{Ag} are the permittivities of Si and Ag, respectively. The permittivity is related to the refractive index through the expression $\sqrt{\varepsilon_X} = n_X$ ($X = Si, Ag$).The dispersion diagram for the geometry shown in Fig. 1 ($h = 200nm$) is displayed in Fig. 2. The TM and TE cavity modes show a dispersion curve that always resides between the air-light line and the Si-light line. Their cut-off is ruled by the intersection with the air-light line. The TM polarization also shows one SPP mode, as expected. As is clear from Fig. 2, this mode is a cavity mode for long wavelengths, and it does not have a cut-off. The mode becomes plasmonic when its dispersion curve crosses the Si-light line. Its phase velocity becomes smaller than the velocity of light in the Si, which means that it can propagate only along directions tangential to the interface while

#157235 - $15.00 USD Received 28 Oct 2011; revised 13 Dec 2011; accepted 16 Dec 2011; published 2 Jan 2012

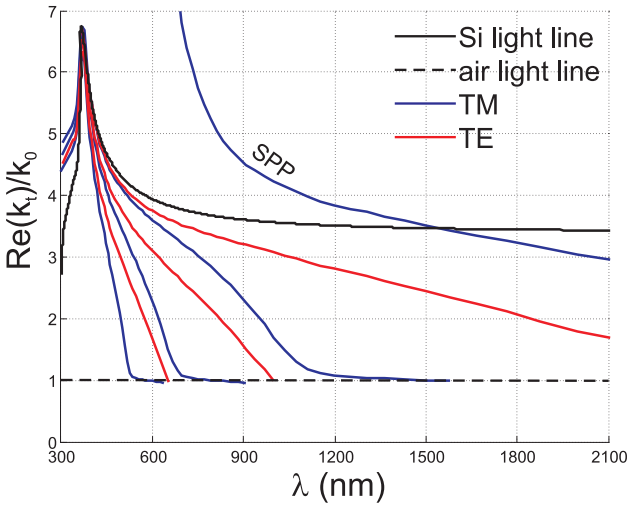

Fig. 2. Dispersion diagram of the flat Ag-Si solar cell. The Si slab has height $h = 200nm$.

attenuating in the longitudinal direction (z). Figure 2 is very useful to elucidate the number of modes supported by the structure that are involved in the light trapping mechanism.

The overall absorption of the solar cell can be calculated as

$$A^p(\lambda) = 1 - |\Gamma^p(\lambda)|^2 \qquad p = \text{TM,TE} \tag{6}$$

where $\Gamma(\lambda)$ is the reflection coefficient at the air-Si interface. The transmission coefficient is neglected because it is negligibly small for these thicknesses. The reflection coefficient can be expressed via the equivalent impedance at the same interface as

$$\Gamma^p(\lambda) = \frac{Z^p_{int} - Z^p_0}{Z^p_{int} + Z^p_0} \qquad p = \text{TM,TE} \tag{7}$$

where Z^p_0 is the TM or TE free space impedance. The calculated absorption is shown in Fig. 3(a) and compared with a full wave simulation performed using CST. The light is impinging normally to the surface, i.e. $k_t = k_0 \sin\theta = 0$ (see Fig. 1), which implies that the two polarizations are equivalent. The structure, in fact, is totally symmetrical. The agreement between the calculated solution from the transmission line model and the full wave result is excellent. We also want to emphasize the spectral nature of the interface impedance, Z_{int}, shown in Fig. 3(b). It is easy to verify that the peaks of absorption occur when the real part of the impedance at the air-Si interface assumes large values and the imaginary part crosses the zero line. This corresponds to an open circuit condition, which implies a peak of the voltage in the equivalent circuit. From the electromagnetic point of view, this behavior reflects a quasi-PMC condition at the interface, justifying a maximum in the tangential electric field, which in turn maximizes penetration inside the Si slab. The peaks shift in the spectrum when the angle of incidence is varied from normal, but the general concepts still hold.

3. Transmission line model of the 1-D grating nanosurface

In this section, we show how to apply the same equivalent transmission line model to a 1-D grating nanosurface. An example of the grating nanosurface is shown in Fig. 4. The ridges have width w, height r, and are in a periodic configuration of period d. The Si has height h. The

#157235 - $15.00 USD Received 28 Oct 2011; revised 13 Dec 2011; accepted 16 Dec 2011; published 2 Jan 2012

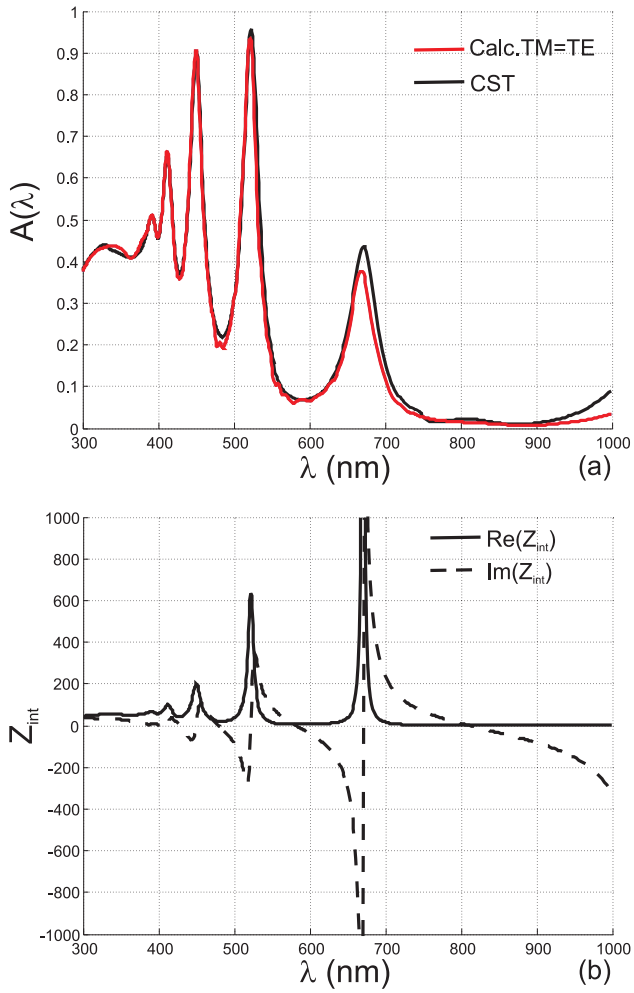

Fig. 3. (a) Calculated absorption compared with a full wave CST simulation for a Si substrate of height $h = 200nm$. The light is impinging normal to the surface, implying that the two polarizations coincide. (b) Equivalent impedance Z_{int} at the air-Si interface calculated through Eq. (2).

#157235 - $15.00 USD Received 28 Oct 2011; revised 13 Dec 2011; accepted 16 Dec 2011; published 2 Jan 2012

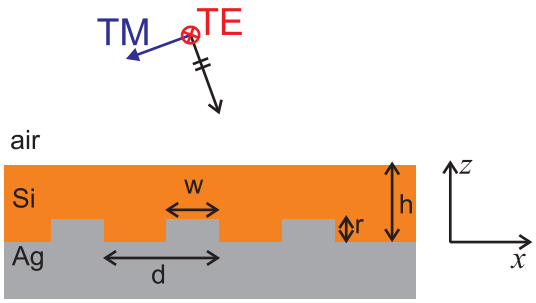

Fig. 4. Reference geometry for the grating nanosurface

conventional TM and TE polarization reference is taken and defined with respect to the plane crossing the grating (*xz* plane). The presence of the ridges introduces additional scattering inside the Si slab, which results in an increase of the photonic and plasmonic path length. A qualitative description of the scattering phenomena is depicted in the top of Fig. 5. The cavity modes are primarily dictated by the reflection of the electromagnetic wave on the metal surface or the ridges of the grating. Furthermore, because of the plasmonic nature of Ag, the light impinging on the edges of the ridge creates an accumulation of positive and negative charge resulting in a dipole-like behavior on each ridge, which is only present for TM polarization. If the ridges are not closely packed, this effect is stronger than the coupling between adjacent ridges. For TE polarization, the electric field is oriented along the edge of the ridges and does not undergo diffraction. This behavior is clear from Fig. 5(a) and (b), where the electric field distribution is shown for both polarizations. In the TM case, the dipole-like electric field appears around the ridge of the grating, while in the TE case, the field distribution is affected just by the reflection mechanism.

The above mentioned phenomena can be interpreted in terms of a transmission line model, as was done for the flat film in Section 2. This leads to an approximate, closed form expression for the total reflection coefficient in Eq. (7), which can be used to calculate the overall absorption from Eq. (6). Although a closed form expression of the absorption coefficient is difficult to obtain for complicated structures, this simple examination of the grating nanosurface is insightful for understanding the basic phenomena. As a first step, we need to calculate the interface impedance, Z_{int}. We use an equivalent transmission line model, which is shown in Fig. 6 and 8 for TE and TM polarizations, respectively. Each unit cell of the grating nanosurface is subdivided into two zones. At the interface between Zone 1 and Zone 2, the tangent component of the electric or magnetic field is continuous. Depending on the polarization, we will use this information to connect the two zones according to the circuit theory.

3.1. Transverse electric excitation

We start with the TE case for simplicity. From Zone 1, we expect to retrieve an equivalent impedance at the interface that can be calculated as in Eq. (2), where here $k_t = k_0 \sin\theta$ and θ is the angle of incidence of the incoming light. We write the transmission line expression again for convenience:

$$Z_1^{TE} = Z_{Si}^{TE} \frac{Z_{Ag}^{TE} + jZ_{Si}^{TE} \tan\left(h\sqrt{k_{Si}^2 - k_0^2 \sin^2\theta}\right)}{Z_{Si}^{TE} + jZ_{Ag}^{TE} \tan\left(h\sqrt{k_{Si}^2 - k_0^2 \sin^2\theta}\right)}. \tag{8}$$

#157235 - $15.00 USD Received 28 Oct 2011; revised 13 Dec 2011; accepted 16 Dec 2011; published 2 Jan 2012

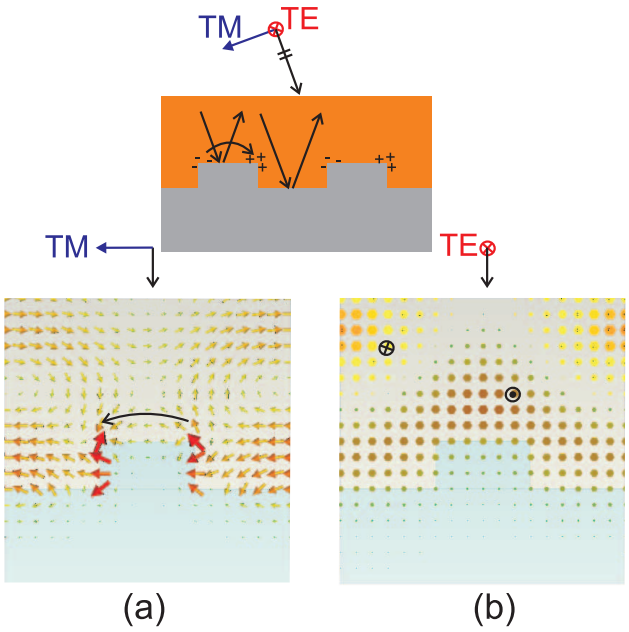

Fig. 5. Qualitative depiction of the scattering process induced by the grating nanosurface (top of the figure). Electric field distribution for normal incidence at $\lambda = 857$ nm: (a) TM polarization; (b) TE polarization.

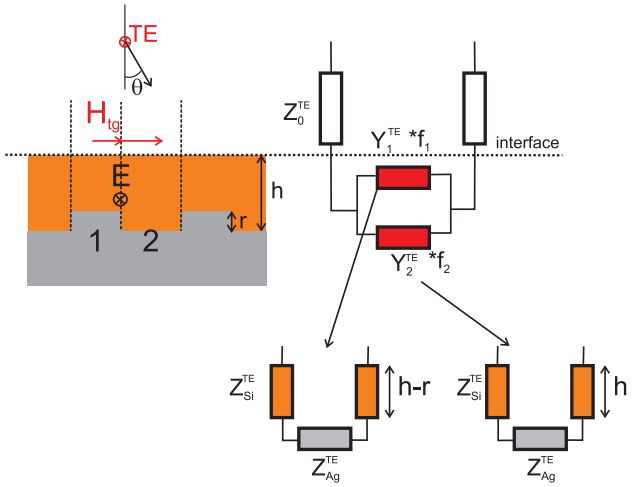

Fig. 6. (left) The unit cell is divided into two main zones, one relevant to the ridge and one relevant to its complementary region. For the TE polarization, the electric field tangent to the junction between the two regions is continuous. This implies that the electric potential difference across the two equivalent loads retrieved at the interface is constant, and the connection is in parallel. (right) TE circuit. The equivalent impedance Z_{int}^{TE} at the interface can be calculated by means of two equivalent admittances at the air-Si interface in a shunt connection weighted by the unit cell filling factors.

#157235 - $15.00 USD Received 28 Oct 2011; revised 13 Dec 2011; accepted 16 Dec 2011; published 2 Jan 2012

For Zone 2, we calculate an equivalent impedance Z_2^{TE} analogous to Z_1^{TE} in Eq. (8), but where the Ag load impedance, Z_{Ag}^{TE}, is moved to the interface by the distance $h-r$ instead of h. For TE polarization, at the junction between Zone 1 and Zone 2, the tangent electric field (tangent to the plane separating the two zones) is always continuous for any angle of incidence (see Fig 6). From a circuit theory point of view, this means that the electric potential difference at the nodes of the two impedances is constant, and the connection between the two loads is then a shunt connection. When dealing with shunt connections, it is easier to express the loads in terms of admittances $Y_{1,2}^{TE} = 1/Z_{1,2}^{TE}$, since the total admittance is simply the sum of the two. To take into account the actual size of Zone 1 and 2 with respect to the unit cell, we weight the two admittances according to unit cell filling factors. In particular, Y_1^{TE} is weighted by a factor $f_1 = w/d$ and Y_2^{TE} by $f_2 = (d-w)/d$. Thus, the equivalent interface impedance to be used in Eq. (7) can be written as

$$Z_{int}^{TE} = \frac{1}{Y_1^{TE} f_1 + Y_2^{TE} f_2} \tag{9}$$

and the absorption can be calculated using Eq. (6). The result for normal incidence ($\theta = 0$) is shown in Fig. 7(a) (red line) along with the full wave CST simulation of the grating nanosurface. The agreement is good overall except for some small discrepancies, which are likely due to higher order effects that are not considered in the model.

3.2. Transverse magnetic excitation

As was done for the TE case, we calculate the equivalent impedance at the air-Si interface from Zone 1 and Zone 2. For Zone 1, we rewrite the Ag load impedance, Z_{Ag}^{TM}, at the interface using the usual transmission line formula (Eq. (8)) applied for TM polarization

$$Z_1^{TM} = Z_{Si}^{TM} \frac{Z_{Ag}^{TM} + jZ_{Si}^{TM} \tan\left(h\sqrt{k_{Si}^2 - k_0^2 \sin^2\theta}\right)}{Z_{Si}^{TM} + jZ_{Ag}^{TM} \tan\left(h\sqrt{k_{Si}^2 - k_0^2 \sin^2\theta}\right)}. \tag{10}$$

For Zone 2, we need to consider two different phenomena. As for Zone 1, there is a Ag load impedance Z_{Ag}^{TM}; however, we must also account for the extra dipole-like contribution due to the TM field diffraction. The latter is dominated by positive and negative charge accumulation at the edge of the ridge, which can be represented as an extra capacitive load in a shunt connection with the Ag load as shown in Fig. 8. We approximate the capacitive impedance associated with this charge accumulation, Z_C, as the series of a capacitance and a resistance (Si has losses)

$$Z_C = \frac{1}{j\omega C} + R_C, \tag{11}$$

with $C = Re(\varepsilon_{Si})w$ and $R_C = Im(\varepsilon_{Si})w$. Then, the impedance Z_2^{TM} is calculated as the parallel of Z_C and Z_{Ag}^{TM} moved to the air-Si interface through the formula in Eq. (10), where Z_{Ag}^{TM} is substituted by the shunt of $Z_{Ag}^{TM} || Z_C$. Moreover, for TM polarization at the junction between Zone 1 and Zone 2, the tangent magnetic field (tangent to the plane separating the two zones) is continuous for any angle of incidence (see Fig 8). From a circuit theory point of view, this means that the current flowing through the two impedances is constant, and the connection between the two loads is then a series connection. The total load is the sum of the two impedances weighted according to the unit cell filling factors, i.e. Z_1^{TM} is weighted by $f_1 = w/d$ and Z_2^{TM} by $f_2 = (d-w)/d$. Thus, the equivalent interface impedance to be used in Eq. (7) can be written as

$$Z_{int}^{TM} = Z_1^{TM} f_1 + Z_2^{TM} f_2 \tag{12}$$

#157235 - $15.00 USD Received 28 Oct 2011; revised 13 Dec 2011; accepted 16 Dec 2011; published 2 Jan 2012

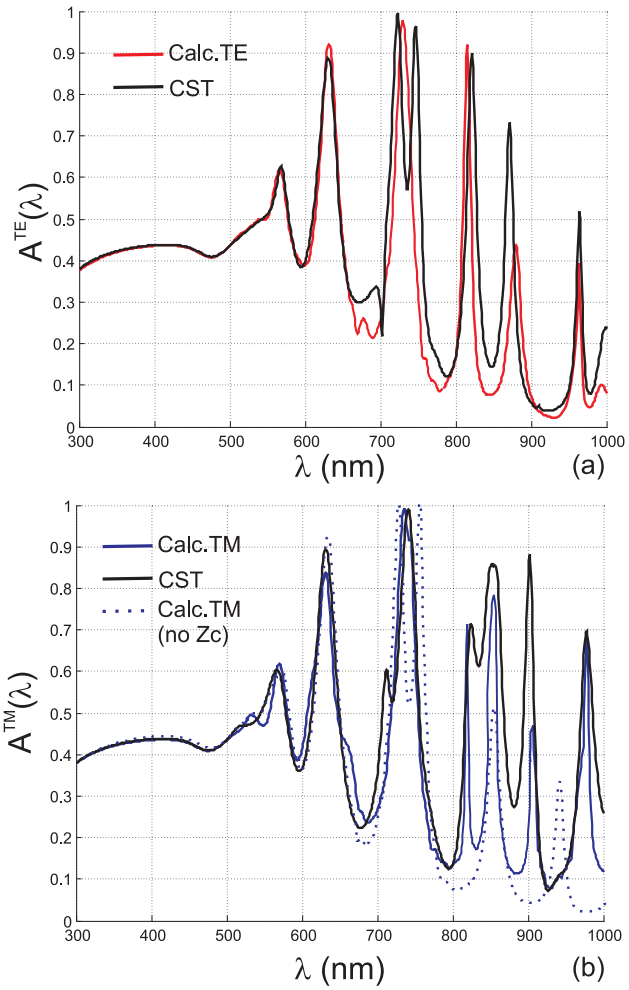

Fig. 7. Comparison of the CST full wave result and absorption calculated with the model for (a) TM and (b) TE excitation for a grating nanosurface with $h = 200nm$, $d = 300nm$, $w = 100nm$, $r = 50nm$.

#157235 - $15.00 USD Received 28 Oct 2011; revised 13 Dec 2011; accepted 16 Dec 2011; published 2 Jan 2012

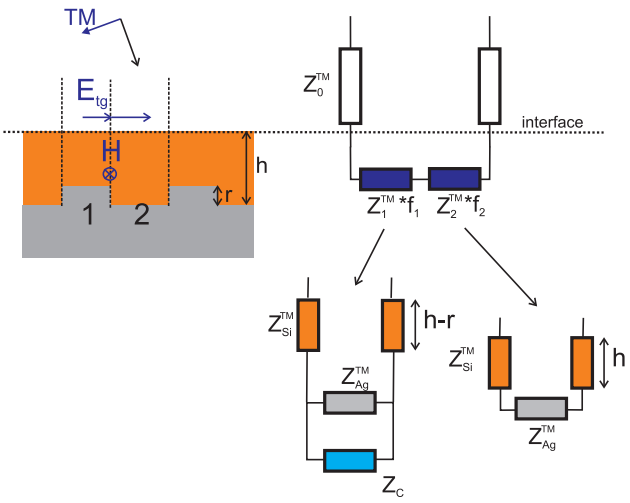

Fig. 8. (left) The unit cell is divided into two main zones, one relevant to the ridge and one relevant to its complementary region. For TM polarization, the magnetic field tangent to the junction between the two regions is continuous. This implies that the current flowing through the two equivalent loads retrieved at the interface is constant, and the connection is in series. (right) TM circuit. The equivalent impedance Z_{int}^{TM} at the interface can be calculated by means of two equivalent impedances at the air-Si interface in a series connection weighted by the unit cell filling factors.

and then the absorption can be calculated through Eq. (6). The result for normal incidence ($\theta = 0$) is shown in Fig. 7(b) (blue line) and compared with a full wave CST simulation. Despite the degree of approximation of the equivalent impedances calculated above, which only account for the largest first order effects, the results show that the global physical mechanism is captured by the model. Also, we show the absorption for the same structure without accounting for the impedance Z_C in the model (dotted line). This result is important because it demonstrates how the plasmonic nature amplifies the diffraction at the ridges of the grating. The calculated absorption without Z_C still agrees with the full wave solution, except in the range of the spectrum where the SPP is strongly excited (see dispersion diagram in Fig. 2).

3.3. Inclusion of an antireflective coating

In most cases, photovoltaic cells are covered by an antireflection (AR) coating (see Fig. 9(a)). The AR coating is a thin layer of dielectric material, whose interference effects cause the wave reflected from the top surface to be out of phase with the wave reflected from the Si surface. These out of phase reflected waves destructively interfere, resulting in zero net reflected energy. This ideal zero-reflection occurs only at the specific frequency and angle of incidence for which its thickness $h_{AR} = \lambda/(4n_{AR}\cos\theta)$, where n_{AR} is the refractive index of the material used as AR coating. We use here TiO_2 with refractive index $n_{AR} = 2.5$ [5] (the material is assumed to be lossless) and set $h_{AR} = 60nm$. We apply the transmission line equivalent circuit model for both TE and TM polarizations, as shown in Fig. 9(b). The equivalent impedance utilized in Section 3.1 for TE and Section 3.2 for TM needs to be transformed by an extra piece of transmission line of length h_{AR} and characterized by a characteristic impedance as in Eq. (1), where $X = AR$. The new Z_{int} impedance is then calculated at the air-AR coating interface using the usual transmission line formula as in Eq. (8) for TE and in Eq. (10) for TM. This result is then plugged into Eq. (7) to evaluate the absorption coefficient analytically via Eq. (6). The

#157235 - $15.00 USD Received 28 Oct 2011; revised 13 Dec 2011; accepted 16 Dec 2011; published 2 Jan 2012

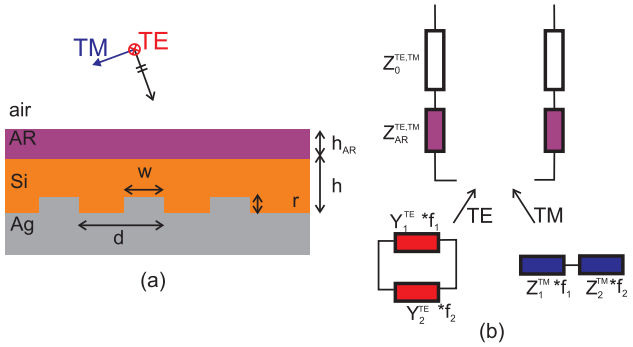

Fig. 9. (a) Reference geometry of the grating nanosurface with a top cover of AR coating. (b) Modification of the transmission line equivalent circuit to account for the extra AR coating.

calculated result is compared with a CST simulation in Fig. 10 for both polarizations. The agreement is extremely good throughout the optical spectrum.

4. Absorption enhancement

Here we will return to the structure without the AR coating to examine the benefits of using a grating structure to increase the effective pathlength. The effective absorption gain of the 1-D grating nanosurface over the flat film solar cell is calculated as

$$G^p(\lambda) = A^p_{grating}(\lambda)/A^p_{flat}(\lambda) \qquad p = \text{TM,TE} \tag{13}$$

where $A_{flat}(\lambda)$ is the absorption for the flat metal film and $A_{grating}(\lambda)$ is for the grating nanosurface. The absorption in each case can be calculated from Eq. (6) and has been shown previously in Figs. 3 and 7 for TE and TM polarizations, respectively. The gain in absorption is shown in Fig. 11(a) for normal incidence. Similar figures have been presented before; however, we want to interpret this result according to our transmission line model. To better understand the nature of the peaks in $G(\lambda)$, we also show the TE and TM equivalent impedance at the air-Si interface compared with the flat film solar cell. In particular, in Fig. 11(b) and (c), the real and imaginary part of Z_{int} is plotted. As described in Section 2, the peaks of absorption occur when the equivalent interface impedance acts like an open circuit, or equivalently the interface acts like a PMC surface. For the grating nanosurface, whenever the equivalent impedance shows a peak in its real part and a crossing of the zero line in its imaginary part, the absorption is maximum. Since we are examining the ratio between the grating absorption and the flat case absorption, the gain shows a substantial increase only when the open circuit condition between the two cases does not overlap. In fact, when it overlaps, the effect is effectively equivalent and leads to an overall cancellation. Also, when the open circuit condition holds only for the flat case, the gain trends toward a minimum. From the plot of $G(\lambda)$ in Fig. 11(a), it is clear that the grating nanosurface has a better performance for the TM polarization. The TM curve shows two main peaks around 750*nm* and 920*nm*, while the TE curve shows only one main peak around 900*nm*. In addition, the TM absorption enhancement peaks are broader in bandwidth. This occurs because the open circuit TE resonances are only due to cavity modes resonances, which are sharp and narrowband. The TM resonances occur as a combination of cavity and plasmonic modes, which improve the gain in both amplitude and bandwidth. As a consequence, better performance is attained when the nanosurface is designed to combine cavity and plasmonic modes to increase the number of open circuit conditions and possibly to increase the bandwidth of the resonances.

#157235 - $15.00 USD Received 28 Oct 2011; revised 13 Dec 2011; accepted 16 Dec 2011; published 2 Jan 2012

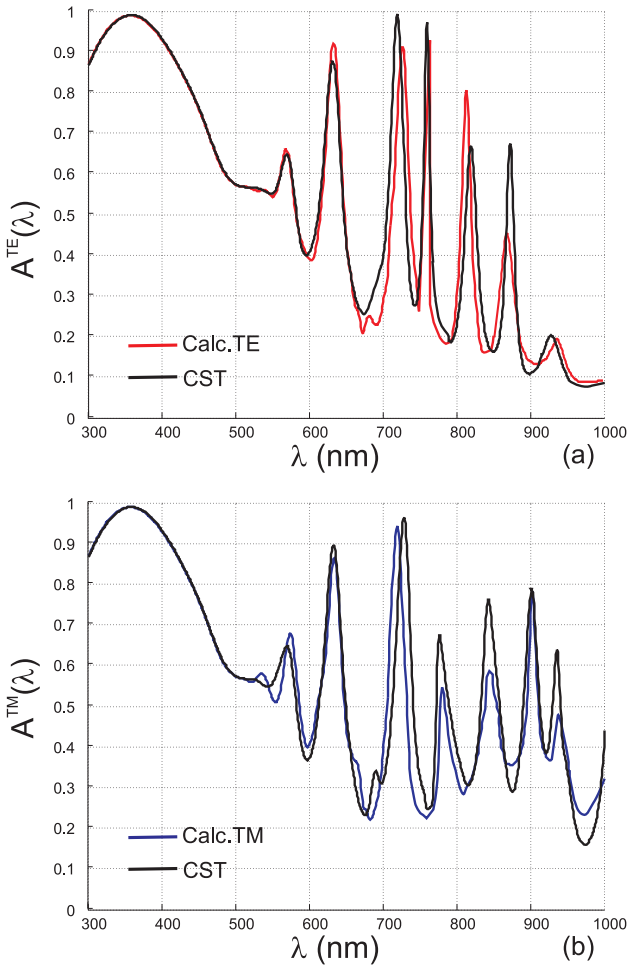

Fig. 10. Comparison of the CST full wave result and absorption calculated with the model for (a) TM and (b) TE excitation for a grating nanosurface with an AR coating of TiO_2. ($h_{AR} = 60nm$, $h = 200nm$, $d = 300nm$, $w = 100nm$, $r = 50nm$.

#157235 - $15.00 USD Received 28 Oct 2011; revised 13 Dec 2011; accepted 16 Dec 2011; published 2 Jan 2012

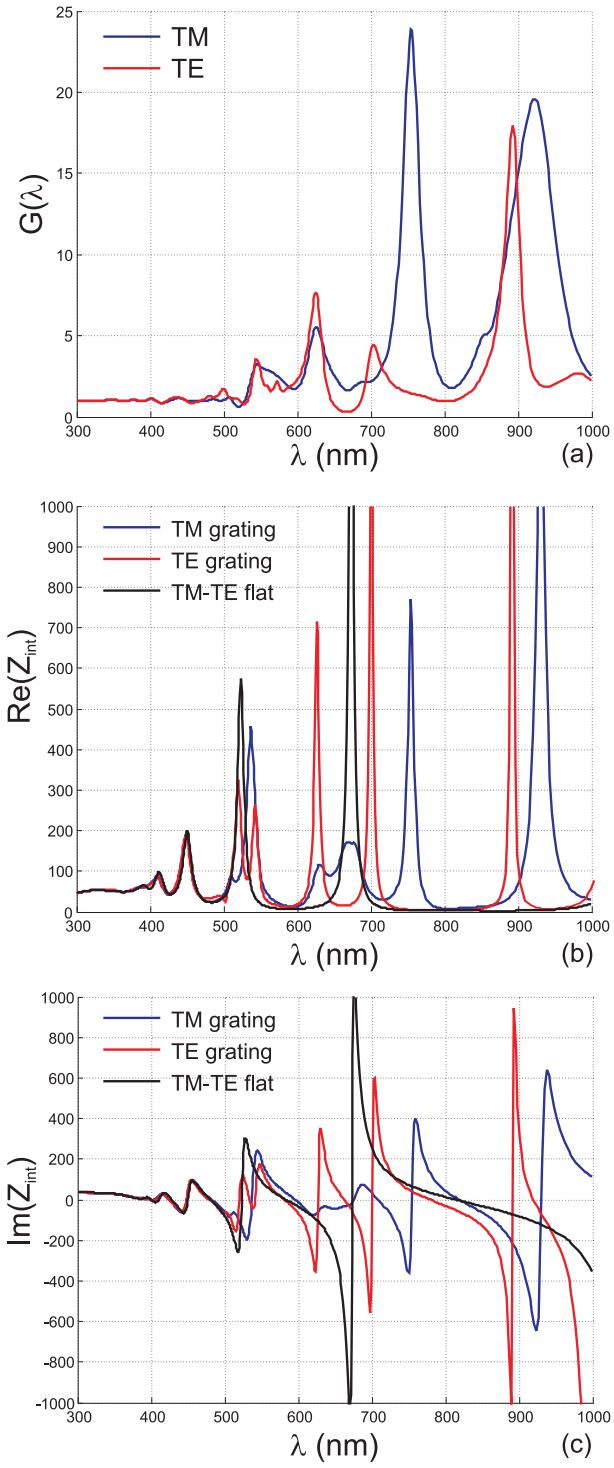

Fig. 11. (a) Absorption gain of the 1-D grating nanostructure over the flat film solar cell for TM and TE polarizations. (b) Real and (c) imaginary part of the equivalent impedance at the air-Si interface for the grating nanosurface and for the flat case.

#157235 - $15.00 USD Received 28 Oct 2011; revised 13 Dec 2011; accepted 16 Dec 2011; published 2 Jan 2012

5. Conclusions

We have shown how light absorption in a plasmonic grating nanosurface can be calculated approximately by means of a simple analytical model based on a transmission line equivalent circuit. The geometry investigated here is a 1-D grating realized on a Ag metal back film covered by a Si slab. The transmission line model is specified for both TE and TM polarizations of the incident light. We have shown how to apply the circuit theory based on the conservation of the tangential components of the electromagnetic field at the junction between the ridge zone and the flat zone of the grating. This has lead to two different connections of elements for TE and TM fields, in particular a shunt connection for the first and a series connection for the second. Also, for the TM polarization, we have included the effect of charge accumulation at the grating ridges by adding an extra capacitive impedance in the circuit to account for plasmon excitation. Under the assumption that the adjacent ridges are not strongly coupled, we have shown that the approximate closed form expression of the reflection coefficient at the air-Si interface can be used to evaluate the light absorption of the solar cell. Moreover, we have demonstrated the utility of the circuit theory as an interpretive tool for understanding peaks in the absorption coefficient and relating these to resonances of the equivalent transmission line model. The weak-coupling assumption employed here is valid if the grating structure is not closely packed and the impinging light is close to normal incidence. We have empirically determined that for the structure under investigation, an angle of incidence beyond 20° from the normal is sufficient to induce higher order couplings, which are not included in the present form of the model. Expanding the model to incorporate higher order effects is under investigation currently. We note in closing that the transmission line model is not meant to substitute for full wave simulations, which are essential for complex nanostructures, but it provides physical insight for understanding the resonances that are responsible for the light trapping mechanism at a fraction of the cost.

Acknowledgments

This material is based upon work supported by the Department of Energy under Award Number DE-SC0006922.

#157235 - $15.00 USD Received 28 Oct 2011; revised 13 Dec 2011; accepted 16 Dec 2011; published 2 Jan 2012